

Nonlinear optical properties of nanometer-size silver coated polydiacetylene composite vesicles and resulting Langmuir–Blodgett films

Xin Chen · Jun Tao · Gang Zou · Wei Su · Qijin Zhang · Shiyong Liu · Pei Wang

Received: 9 April 2010 / Accepted: 29 September 2010 / Published online: 20 October 2010
© Springer-Verlag 2010

Abstract Noble metal-coated PDA composite vesicles were expected to increase the effective third-order nonlinear optical susceptibility $\chi^{(3)}(\omega)$, due to the enhancement of the optical electric field induced by localized surface plasmon resonance. Different size (20, 50 and 80 nm) Ag colloidal nanoparticles were coated on the outer surface of polydiacetylene (PDA) vesicles to form PDA/Ag nanocomposite vesicles and the size-dependent effect of Ag colloidal nanoparticles on NLO properties enhancement has been explored. The explanation based on the competition of a size-dependent light-confinement effect and a size-dependent dielectric constant of Ag particles had been presented. Furthermore, these PDA/Ag composite vesicles were successfully immobilized onto the solid substrate by the Langmuir–Blodgett (LB) method and their linear and nonlinear optical properties were characterized, respectively. Obviously, PDA/Ag composite vesicles Langmuir–Blodgett (LB) films promoted the enhancement of the third-order NLO properties.

Electronic supplementary material The online version of this article (doi:10.1007/s00339-010-6071-8) contains supplementary material, which is available to authorized users.

X. Chen · G. Zou (✉) · W. Su · Q. Zhang · S. Liu
CAS Key Laboratory of Soft Matter Chemistry, Department of Polymer Science and Engineering, Key Laboratory of Optoelectronic Science and Technology in Anhui Province, University of Science and Technology of China, Hefei, Anhui 230026, China
e-mail: gangzou@ustc.edu.cn
Fax: +86-551-3601704

J. Tao · P. Wang
Department of Physics, Key Laboratory of Optoelectronic Science and Technology in Anhui Province, University of Science and Technology of China, Hefei, Anhui 230026, China

1 Introduction

During the past decade, much significant research has been directed toward understanding organic nonlinear optical (NLO) materials and their application in information processing due to their large NLO response and short response time [1]. Among these organic NLO materials, polydiacetylene (PDA), classified as a one-dimensional π -conjugated polymer, possesses excellent third-order NLO response properties in the range of femtoseconds to sub-picoseconds, which is attributed to delocalized π -conjugated electrons along the main chain backbone [2]. PDA can be chemically tailored by means of polymerization reaction in solid phase of a substituted mono diacetylene. Many theoretical and experimental efforts have been made to improve the effective third-order NLO susceptibility $\chi^{(3)}(\omega)$ of PDA system. Among them, the extension of π -conjugation between main chain and side chains is a fairly attractive technique, such as directly linked aromatic groups and ladder-type PDAs [3, 4]. An alternative approach is to fabricate nanocomposites with well-defined shape holding improved NLO properties. Therefore, metallic nanoparticles have attracted lots of interest for their fascinating optical and electronic properties [5]. With the particle size reaching the nanometer scale, not only the surface-to-volume ratio drastically changes but a transition from metal to insulator also occurs, resulting from quantum confinement [6]. The surface plasma resonance (SPR), which results from collective electronic excitation at the interface between metal nanoparticles and dielectric matrix, not only is responsible for the linear optical properties but also governs nonlinear optical phenomena [7]. By incorporating metal nanoparticles into a organic NLO materials matrix [8–10], the nanocomposite films have attractive mechanical and electronic properties that facili-

tate their use in the practical devices and have been regarded as the potential materials for all-optical communication.

According to the local-field enhancement under the surface plasmon resonance condition, larger third-order nonlinearity of polydiacetylene composite films has been observed in the presence of metal or semiconductor nanoparticles [11–14]. Neeves and Birnboim theoretically predicted that the core-shell-type structure consisting of a PDA core and a metal nanoshell exhibits markedly large effective $\chi^{(3)}(\omega)$ values [15], which encourages people to develop many novel types of core-shell-type nanoparticles [16–20]. This enhancement in $\chi^{(3)}(\omega)$ relies both on the optical field concentration at each nonlinear medium and on plasmon resonance at the interface. For example, in case of PDA microcrystal (core) and gold (shell) hybridized microparticle, $\chi^{(3)}(\omega)$ in e.s.u. unit would be expected to be about 100 times larger compared to pure PDA microcrystal [21]. In our previous work [22], we reported the fabrication of PDA/Ag nanocomposite vesicles and firstly experimentally demonstrated the enhancement of third-order NLO properties as a result of the surface plasmon resonance of silver nanoparticles at the interface. The NLO properties of nanometer-size metal particles embedded in dielectric material can be modulated by varying the size [23], shape [24, 25] and the volume fraction [26] of metal nanoparticles because of the changing of the local surface plasmon resonances field outside the metal particles. From the practical point of view, these parameters can be optimized to meet optical device operation. In this paper, the size-dependent effect of Ag colloidal nanoparticles on NLO properties enhancement had been explored to optimize the structural parameters of the PDA/Ag nanocomposite vesicles.

Immobilization of PDA vesicles onto thin films would enhance their storage stability and user-friendliness. Despite long and extensive research on PDA vesicles, reports on the fabrication of films containing these materials have just come to light in recent years [27, 28]. Immobilization of PDA/Ag nanocomposite vesicles onto solid substrate and the network aggregates formation of PDA/Ag nanocomposite vesicles are expected to enhance their NLO properties and stability, which are very important for the potential application in NLO devices. To the best of our knowledge, the direct assemblies of these PDA/Ag nanocomposite vesicles and characterization of their NLO properties have not yet been successful. In this paper, the above optimized PDA/Ag nanocomposite vesicles would be immobilized on the solid substrate and their NLO properties are expected to be enhanced further. The strategy described in this work would be useful in the development of new PDA-based optical and NLO devices.

2 Experimental section

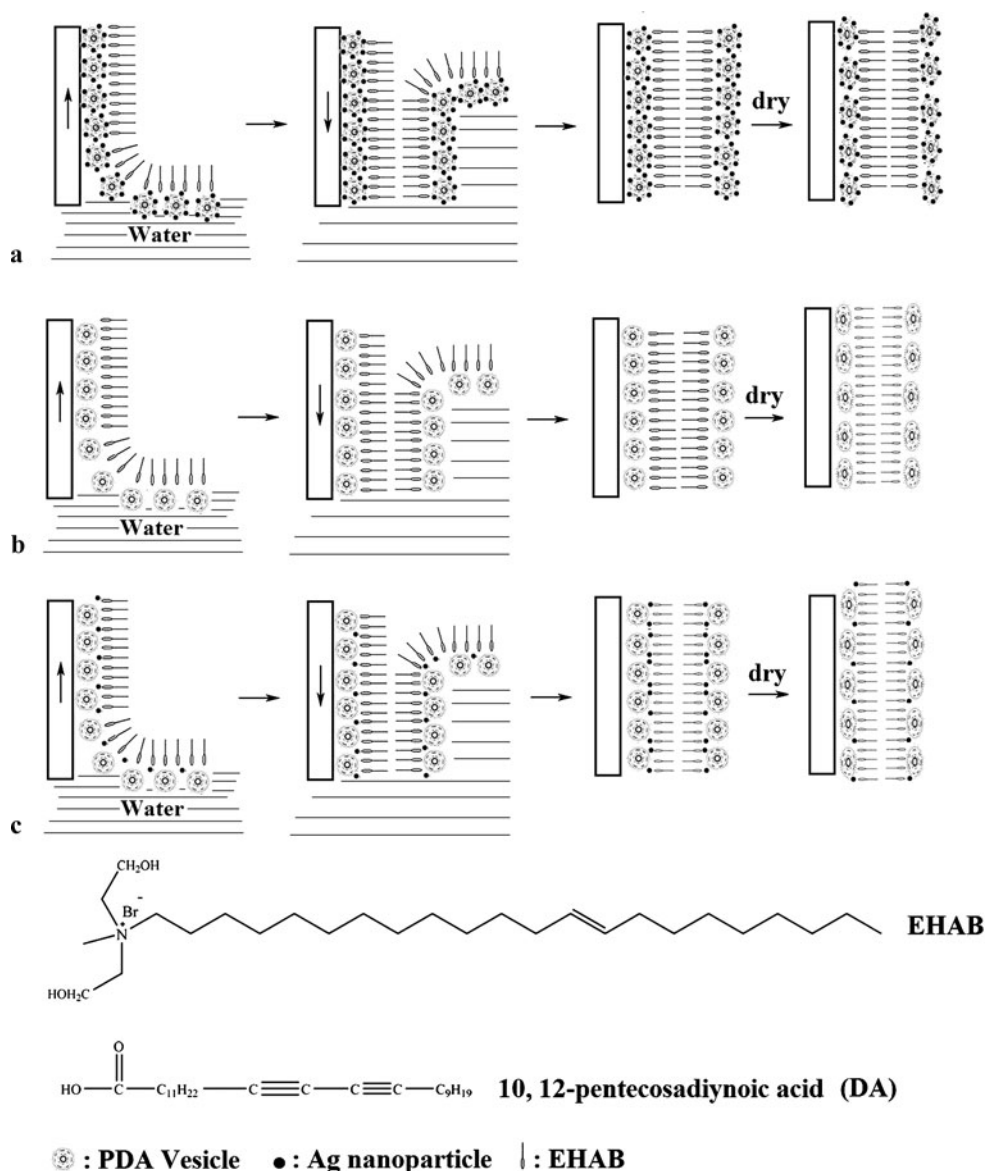
Materials. AgNO_3 , NaBH_4 and trisodium citrate were obtained from Beijing Chemical Reagent Ltd and used without further purification. 10, 12-pentacosadiynoic acid ($\text{CH}_3-(\text{CH})_{11}-\text{C}\equiv\text{C}-\text{C}\equiv\text{C}-(\text{CH})_8-\text{COOH}$, DA) was purchased from Tokyo Chemical Industry Co. Ltd., and purified by dissolving in cyclopentanone and filtrating to remove polymer before use. N,N-bis(2-hydroxyethyl)-N-methyl-N-(Z-13-docosyl)quaternary ammonium bromide (EHAB) was synthesized in analogy to the previous procedure [29]. The molecular structures of DA and EHAB were shown in Fig. 1.

Fabrication of PDA/Ag nanocomposite vesicles. PDA/Ag nanocomposite vesicles were prepared according to the same procedure described in literature [22]: Well-defined PDA vesicles cores were firstly prepared by the conventional method [27, 28]. Then different size (20, 50 and 80 nm) Ag colloidal nanoparticles were coated on the outer surface of PDA vesicles through strong electrostatic interaction between the carboxyl group of PDA vesicles and Ag colloidal nanoparticles. The size dispersion of the Ag colloidal nanoparticles was characterized by Dynamic Light Scattering (DLS). The preparation process was monitored by UV-vis absorption analysis. The structure of PDA/Ag nanocomposite vesicles were characterized by TEM analysis.

LB films of PDA/Ag composite vesicles. Glass substrates were cleansed of organic contaminants by 15 min boiling in an oxidizing “piranha” solution prepared by mixing a 3:1 volume ratio of concentrated sulfuric acid with hydrogen peroxide solution (30%). A Langmuir–Blodgett trough (KSV mini, Finland) was used for deposition of LB films. Surface pressure was measured with a platinum Wilhelmy plate. An EHAB solution in chloroform (2.11×10^{-3} mol/L) was used as the spreading solution. The aqueous solution of PDA vesicles, PDA/Ag composite vesicles or PDA vesicles mixed with negative charged Ag nanoparticles (5×10^{-5} mol/L, prepared according to the same procedure as described in literature [22]) were respectively used as subphase and the temperature was maintained at 22°C. After evaporation for 20 min, the surface was compressed slowly to record the pressure–area isotherm. A compression rate of 5 mm/min was used for studying the pressure–area isotherm. When the desired surface pressure was attained, the monolayers were transferred from the air–water interface to a solid substrate (glass slides) by LB method. A surface pressure of 25 mN/m was maintained for deposition of LB films and 80 monolayers were deposited. Dipping and raising speed was fixed at 5 mm/min and a waiting time of 10 min was given between dips to dry the LB film (as shown in Fig. 1).

Characterization. Transmission electron microscopy (TEM) image were recorded on a JEOL-2000 microscope

Fig. 1 a Schematic preparation of PDA/Ag nanocomposite vesicles LB films of a EHAB and PDA/Ag nanocomposite vesicles (reference sample), b EHAB and pure PDA vesicles, c EHAB, Ag nanoparticles (Negative charge) and pure PDA vesicles



operated at 200 kV. For the TEM observation, samples were obtained by dropping 5 μ l of solution onto carbon-coated copper grids. All the TEM images were visualized without staining. All ultraviolet-visible (UV-vis) spectra were measured using a SHIMADZU UV-2550 PC spectrophotometer. The linear refractive index of solution samples were measured by Abbe refractometer (ATAGO NAR-1T). The linear refractive indexes of LB films were measured by Ellipsometer (ELLIP-SR). The surface morphology and thicknesses of LB films were studied by Atomic Force Microscope (nanoscope IIIa). All NLO properties of samples were investigated by Z-scan technique, using 100 μ J pulse energy, 16 ns pulse duration and 10 Hz repetition rate at 532 nm, available from a frequency-doubled Q-switched Nd: YAG laser (Quantum YAG 980). The Z-scan experiments were done at the average intensity level of 0.4 GW/cm². The so-

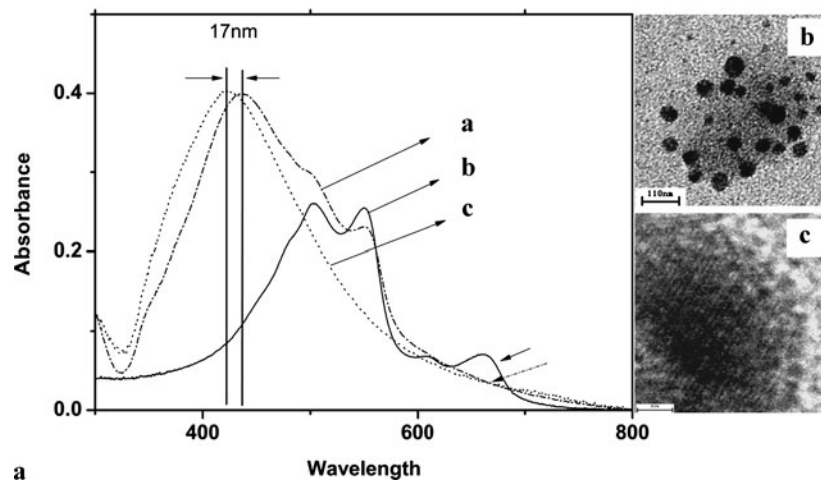
lution sample in a 1 mm thick quartz cell and film samples on quartz substrates were moved along the Z axes close to the focus of the lens, which had a focal length of 26 cm. The concentration of the solution samples used in Z-scan experiments was the same as those used in UV-vis spectrum experiments. The transmitted beam energy, the reference beam energy and their ratio were monitored by the energy meters (EPM 2000), simultaneously.

3 Results and discussion

3.1 Preparation of PDA/Ag nanocomposite vesicles with different size Ag colloidal nanoparticles

The preparation process of PDA/Ag nanocomposite vesicles was monitored by UV-vis absorption analysis. The size and

Fig. 2 **a** UV-vis optical absorption spectra of (i) 50 nm Ag colloidal nanoparticles, (ii) PDA vesicles and (iii) PDA/Ag (50 nm) composite vesicles, **b** TEM images (the scale bar is 200 nm) and **c** HRTEM images (the scale bar is 4 nm) of PDA/Ag (50 nm) composite vesicles



size distribution of Ag nanoparticles was confirmed by Dynamic Light Scattering (DLS) (as shown in Fig. S3 in electronic supplementary material). Although the distributions are all a little broad (20 nm Ag nanoparticles: 10–50 nm; 50 nm Ag nanoparticles: 35–100 nm; 80 nm Ag nanoparticles: 55–115 nm), the majority of nano-silver particles are in the size of 20, 50 and 80 nm, respectively. The size of Ag colloidal nanoparticles also could be confirmed directly by transmission electron microscopy (TEM). The structure of these nanocomposite vesicles was investigated by means of TEM and high resolution transmission electron microscopy (HRTEM). In our previous work [22], we reported that PDA/Ag (20 nm) composite vesicles solution was successfully fabricated. Here we prepared PDA/Ag (50 and 80 nm) composite vesicles solution and further investigated the size-dependent effect of Ag colloidal nanoparticles on NLO properties enhancement of PDA/Ag composite vesicles. The UV-vis absorption spectra of 50 nm Ag colloidal nanoparticles, pure PDA vesicles and PDA/Ag (50 nm) composite vesicles solution were shown in Fig. 2a. The 50 nm Ag colloidal nanoparticles had an absorption peak located at about 419 nm, which resulted from the surface plasmon resonant oscillation of the free electrons in metal Ag. Pure PDA vesicle had three characteristic absorption peaks at about 650, 550 and 500 nm and it had a vesicles shell structure about 100 nm in diameter characterized by TEM. When Ag colloidal nanoparticles solution was dipped into PDA vesicles solution, obvious optical change could be observed. After mixing, the peak position of Ag nanoparticles located at about 419 nm shifted to 436 nm when Ag nanoparticles attached onto the outer surface of PDA vesicles, giving evidence that the isolated silver nanoparticles with the carboxyl group had been coated onto the surface of PDA vesicles. The width of the surface plasma absorption band of silver nanoparticles became broad after mixing. The absorption peak of PDA vesicles at about 650 nm decreased a lot, giving another evidence of the coating of

isolated silver nanoparticles with the carboxyl group on the surface of PDA vesicles. When the Ag nanoparticles coated on the outside of PDA vesicles, the interaction between Ag nanoparticles and PDA side chains can release the side chains strain and induce a partial distortion of the conjugated p-orbital arrays, leading to the shortening of effective p-conjugation length. Thus PDA would transform from blue to red form, which go with the decreasing of blue absorption peak of PDA vesicles at about 650 nm. The TEM images are displayed in Fig. 2b, which demonstrates the formation of PDA/Ag (50 nm) nanocomposite vesicles. The HRTEM images, displayed in Fig. 2c, indicate that there was not a perfect silver crystalline plane, and the plane distance was about 3 Å. All these above results indicated that PDA/Ag (50 nm) nanocomposite vesicles were prepared successfully. Similarly, the analysis of UV-vis absorption spectra, TEM and HRTEM images (as shown in Fig. 3) demonstrate that PDA/Ag (80 nm) nanocomposite vesicles were prepared successfully.

3.2 NLO characterization of PDA/Ag nanocomposite vesicles

To evaluate the size-dependent effect of Ag colloidal nanoparticles on NLO properties enhancement, different size Ag colloidal nanoparticles (20, 50 and 80 nm) were used to prepare PDA/Ag nanocomposite vesicles. NLO properties of PDA/Ag composite vesicles with different size of Ag nanoparticles (20, 50 and 80 nm) have been evaluated by means of a Z-scan technique. Open and closed aperture Z-scan measurements were used to evaluate the nonlinear refraction and nonlinear absorption properties. Figure 4 showed the Z-scan curves of pure PDA vesicles solution and PDA/Ag (20, 50 and 80 nm) nanocomposite vesicles solution, respectively. The nonlinear refractive index n_2 and the nonlinear absorption coefficient β were measured according

Fig. 3 **a** UV-vis optical absorption spectra of (i) 80 nm Ag colloidal nanoparticles, (ii) PDA vesicles and (iii) PDA/Ag (80 nm) composite vesicles, **b** TEM images (the scale bar is 110 nm) and **c** HRTEM images (the scale bar is 4 nm) of PDA/Ag (80 nm) composite vesicles

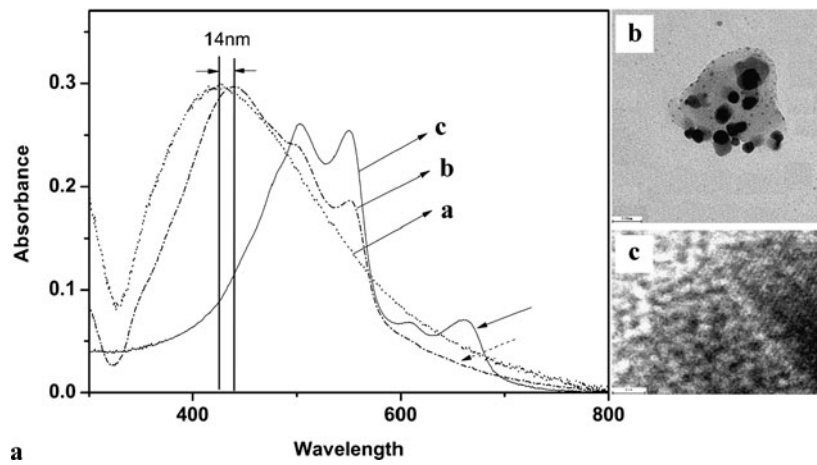
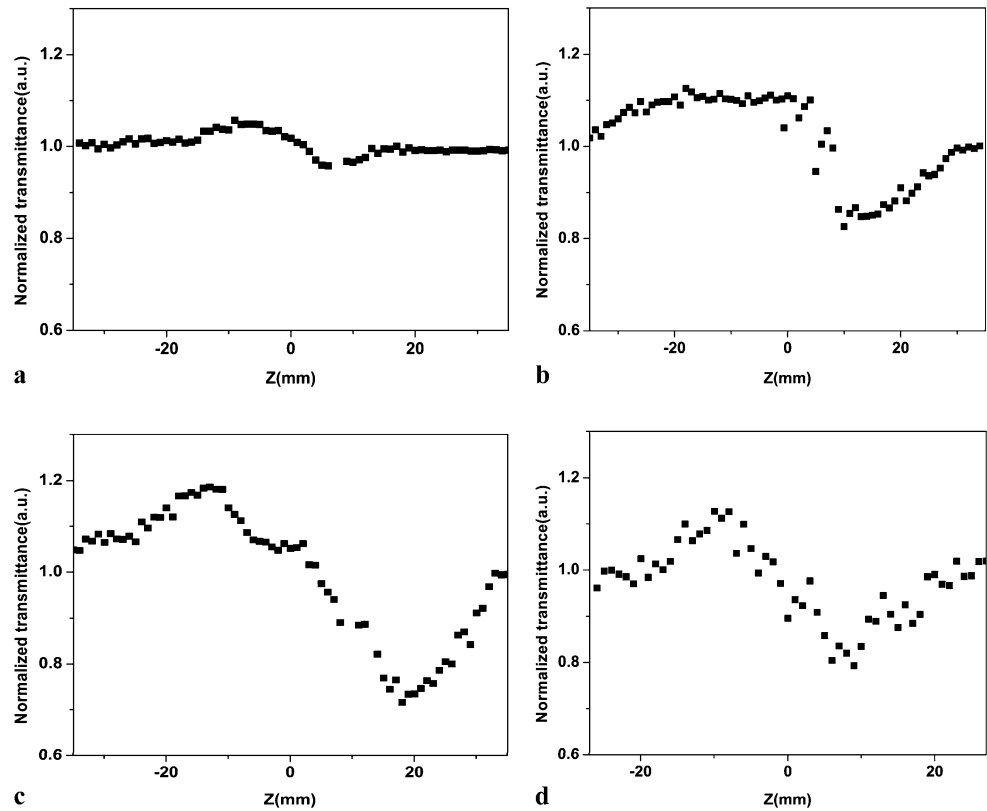


Fig. 4 Measured Z-scan normalized transmittance curves of **a** pure PDA vesicles solution, **b** PDA/Ag (20 nm) composite vesicles solution, **c** PDA/Ag (50 nm) composite vesicles solution and **d** PDA/Ag (80 nm) composite vesicles solution



to the following equations [30]:

$$n_2 = \gamma = \frac{\Delta T_{p-v}}{k I_0 L_{\text{eff}} 0.406 (1 - S)^{0.25}} \quad (1)$$

$$T(z, S = 1) = 1 - \frac{\beta I_0 L_{\text{eff}}}{2\sqrt{2}(1 + (z/z_0)^2)} \quad (2)$$

where $k = 2\pi/\lambda$ is the wave vector, I_0 is the on-axis irradiation of the laser beam at focus ($z = 0$), $L_{\text{eff}} = 1 - \exp(-\alpha L)/\alpha$ is the effective thickness with L the sample thickness, S is the aperture linear transmittance, α is the linear absorption coefficient, z is the position of the sam-

ple and $z_0 = k\omega_0^2/2$ is the diffraction length of the beam. The peak-valley configuration indicates the nonlinear refraction was negative and belonged to self-defocusing nonlinearity. The linear absorbance at 532 nm and the linear absorbance coefficient for PDA/Ag (20, 50 and 80 nm) nanocomposite vesicles were 0.34, 0.31, 0.33, 3.4 cm^{-1} , 3.1 cm^{-1} , and 3.3 cm^{-1} , respectively. The nonlinear refractive index and the nonlinear absorption coefficient were measured to be $2.47 \times 10^{-14} \text{ cm}^2/\text{W}$, $4.3 \times 10^{-14} \text{ cm}^2/\text{W}$, $2.94 \times 10^{-14} \text{ cm}^2/\text{W}$, $5.6 \times 10^{-11} \text{ m/W}$, $10.2 \times 10^{-11} \text{ m/W}$, and $8.1 \times 10^{-11} \text{ m/W}$, respectively. The resulting $\chi^{(3)}(\omega)$ are calculated to be $0.94 \times 10^{-12} \text{ esu}$, $1.63 \times 10^{-12} \text{ esu}$, and

Table 1 Nonlinear refractive index n_2 , $\chi^{(3)}$ and nonlinear absorption coefficient β for different PDA/Ag nanocomposite vesicles solution and resulting LB films

Samples		n_2 ($\times 10^{-13}$ cm ² /W)	R_3 ($\times 10^{-11}$ esu)	β ($\times 10^{-11}$ m/W)
PDA/Ag composite vesicles solution	Pure PDA vesicles solution	0.04	0.01	2.5
	Solution I (20 nm Ag nanoparticles coated onto the outer surface of PDA vesicles)	0.2	0.09	5.6
	Solution II (50 nm Ag nanoparticles coated onto the outer surface of PDA vesicles)	0.4	0.2	10.2
	Solution III (80 nm Ag nanoparticles coated onto the outer surface of PDA vesicles)	0.3	0.1	8.1
PDA/Ag composite vesicles L–B film	Pure PDA vesicles LB film	9.16	7.1	45.3
	PDA vesicles mixed with Ag nanoparticles (50 nm, negative charge) L–B film	28.1	23.0	58.9
	PDA/Ag (50 nm, positive charge) composite vesicles L–B film	58.2	53.0	147

1.12×10^{-12} esu, respectively. All the values of n_2 , $\text{Re}\chi^{(3)}$ and nonlinear absorption coefficient for different samples were listed in Table 1. There is a decrease in the value of n_2 while going from a solution with low absorbance of 0.31 (PDA/Ag (50 nm) composite vesicles), 0.33 (PDA/Ag (80 nm) composite vesicles), and 0.34 (PDA/Ag (20 nm) composite vesicles) to a solution of high absorbance of 0.40 (pure PDA vesicles). It clearly indicated that n_2 was predominantly electronic in origin rather than due to thermal nonlinearity. If the thermal contributions were dominating, one should obtain an increase in n_2 with increasing of absorption. Nearly 13 times enhancement in the effective third-order NLO susceptibility $\chi^{(3)}(\omega)$ was observed for PDA/Ag (50 nm) composite vesicles, however, only seven times and nine times enhancement were observed for PDA/Ag (20 and 80 nm) composite vesicles, respectively. This NLO properties enhancement was attributed to the local-field enhancement under the surface plasmon resonance of silver nanoparticles at the interface. The formation of core-shell-type structure consisting of a PDA vesicle core and an Ag nanoshell (Ag colloidal nanoparticles were coated onto PDA vesicles, not simply mixing) was proven to be essential for this remarkable NLO properties enhancement [22]. All above results were in agreement with the theoretical prediction of Neeves [15] and our previous experimental results [22]. Obviously, PDA/Ag (50 nm) composite vesicles showed maximum NLO properties enhancement effect. This size-dependent enhancement effect of Ag colloidal nanoparticles should be attributed to two size-dependent factors:

light-confinement and dielectric constant. The competition of a size-dependent light-confinement and a size-dependent dielectric constant of Ag spheres determined the enhancement factor E_{out}/E_0 . Thus there should be an optimum size of Ag particles at which the largest NLO property enhancement will occur.

The field outside the sphere E_{out} was measured according to the following equations [31]:

$$E_{\text{out}} = E_0 \hat{x} - \alpha E_0 \left[\frac{\hat{x}}{r^3} - \frac{3x}{r^5} (x\hat{x} + y\hat{y} + z\hat{z}) \right] \quad (3)$$

where α is the sphere polarizability, and \hat{x} , \hat{y} and \hat{z} are the usual unit vectors. We note that the first term in (3) is the applied field and the second is the induced dipole field (induced dipole moment = αE_0), which results from polarization of the conduction electron density.

The polarizability is

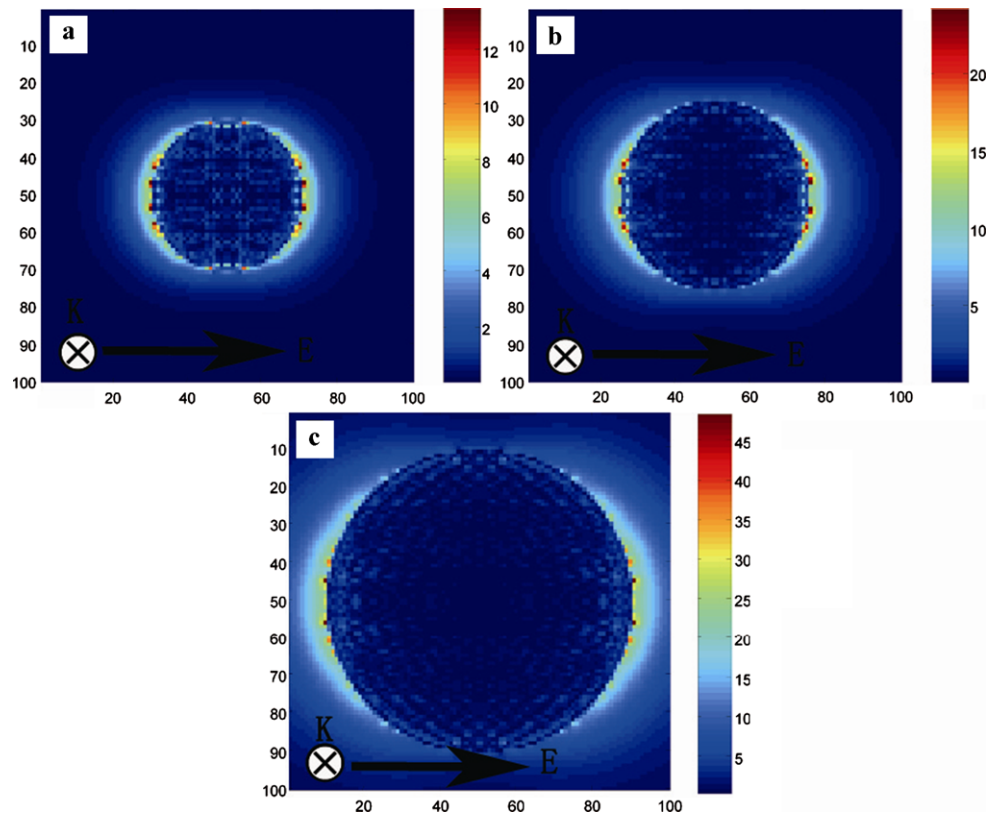
$$\alpha = g_d (D/2)^3 \quad (4)$$

with

$$g_d = \frac{\varepsilon_i - \varepsilon_0}{\varepsilon_i + 2\varepsilon_0} \quad (5)$$

where D is the diameter of the Ag sphere, ε_i and ε_0 are the wavelength-dependent dielectric constant of Ag nanoparticles and the dielectric constant of the surrounding medium, respectively. In order to observe this field enhancement directly, we simulated the local field of different size Ag

Fig. 5 The simulation of the local field of **a** 20 nm Ag nanoparticle, **b** 50 nm Ag nanoparticle, **c** 80 nm Ag nanoparticle



nanoparticles by the discrete dipole approximation (DDA) method (as shown in Fig. 5). We found that the local field outside the sphere E_{out} enhanced with increasing of the diameter of Ag spheres. Above simulation results are not very consistent with our experimental findings, because we assumed the dielectric constant of the different size of Ag nanoparticles to be constant in the simulation process. Actually, the dielectric constant of small-size Ag spheres showed a strong size dependence and the imaginary part of $\varepsilon(\omega, \alpha)$ is even stronger affected by the size of Ag spheres [32]. Thus, both the effect of the size-dependent light-confinement and the size-dependent dielectric constant of Ag spheres both must be considered. The influence factor of nonlinear effect E_{out}/E_0 was dependent on the size of silver nanoparticles and the maximum of E_{out}/E_0 arises from competition of Ag size-dependent optical confinement and Ag size-dependent optical loss. The variation of the refractive index due to the Kerr effect should, therefore, be largest at $D = 40$ nm. As a consequence, E_{out}/E_0 becomes maximum at $D = 40$ nm [33]. This theoretical calculation using modified Mie theory is well in agreement with our experimental results that PDA/Ag (50 nm) composite vesicles showed maximum NLO properties enhancement effect. This size-dependent enhancement effect could be attributed to the competition of a size-dependent light-confinement and a size-dependent dielectric constant of Ag spheres.

3.3 Characterization of PDA/Ag nanocomposite vesicles LB films

Immobilization of PDA/Ag nanocomposite vesicles onto solid substrate and the network aggregates formation of PDA/Ag nanocomposite vesicles have been expected to enhance their NLO properties and stability, which are very important for the potential application in NLO devices. Here, PDA/Ag (50 nm) composite vesicles were immobilized onto the solid substrate by LB methods. EHAB solution was used to form monolayer at air/water interface and PDA/Ag (50 nm) composite vesicles solution was used as the sub-phase. PDA/Ag (50 nm) composite vesicles can be adsorbed onto the EHAB monolayer due to the electrostatic interaction (negatively charged vesicles and positively charged monolayer molecules). UV-vis absorption spectrum was employed to monitor the LB assembly process. An absorption peak at 436 nm (the characteristic absorption of Ag), 550 nm and 500 nm (the characteristic absorption of PDA) can be seen for the resulting of LB films (as shown in Fig. 6a), which indicated that PDA/Ag (50 nm) composite vesicles did deposit onto the substrate. The good linearity between the number of layers and the absorbance at 550 nm (as shown in Fig. 6b) indicates that the PDA/Ag nanocomposite vesicles have incorporated with EHAB monolayer and can be successively and regularly deposited layer by layer during the whole deposition process. X-ray diffraction stud-

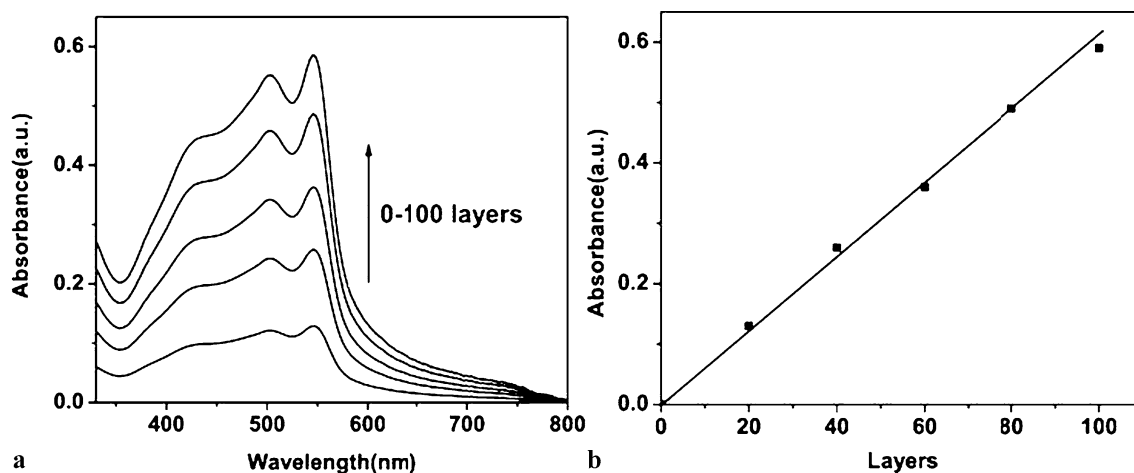


Fig. 6 **a** UV-vis optical absorption spectra of LB films composed of PDA/Ag (50 nm, positive charge) composite vesicles. **b** Absorbance at 550 nm of LB films composed of PDA/Ag (50 nm, positive charge) composite vesicles as a function of the number of layers

ies indicated that the preparation of EHAB LB films as described above with PDA/Ag (50 nm) composite vesicles subphase was successful. The appearance of five equidistant Bragg diffraction peaks in the range $2\theta = 1.2^\circ \sim 10^\circ$ indicated the presence of a regular, periodic structure in the LB film. The average spacing in the LB film on glass slide could be calculated to be about 7 nm (as shown in Fig. 7). In general, vesicles change their aggregate morphology by collapse and fusion in contact with solid surfaces to form supported membranes. The formation of supported membranes relative to that of vesicles depends on competition between the adhesive energy and the vesicle bending energy [25]. AFM was utilized to characterize the morphology of above PDA/Ag (50 nm) composite vesicles LB films upon quartz substrate surface. A remarkably rough surface was observed and the non-regular approximate spherical particles, whose sizes are approximately 150–300 nm, were clearly seen in the AFM images (as shown in Fig. 8). However, the thickness of above non-regular particles is about 10 nm, which is in accordance with the results of XRD. It should be ascribed to the collapse and shrinkage of PDA/Ag nanocomposite vesicles after immobilization and drying. Despite a certain degree of collapse, all above results indicated that PDA/Ag nanocomposite vesicles retained their structure and shape after immobilization. Similarly, the aqueous solution of PDA vesicles and PDA vesicles mixed with negatively charged Ag nanoparticles with the same concentration were used as the subphase. LB films of PDA vesicles and PDA vesicles mixed with negative charged Ag nanoparticles could be fabricated as the reference sample.

NLO properties of LB films of PDA/Ag nanocomposite vesicles, pure PDA vesicles and PDA vesicles mixed with negatively charged Ag nanoparticles had been evaluated by means of a Z-scan technique as shown in Fig. 9. The linear absorbance at 532 nm and linear absorbance co-

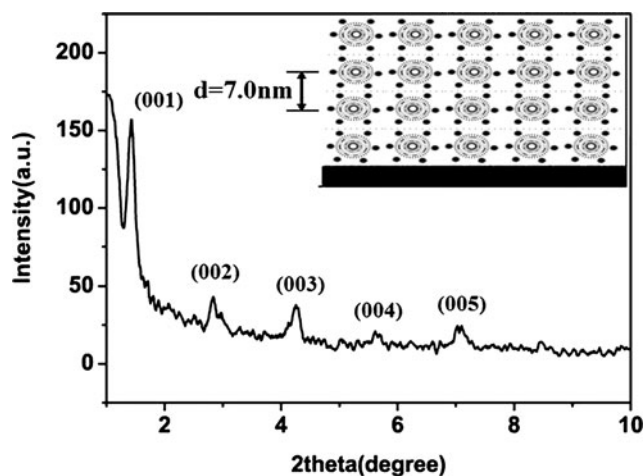


Fig. 7 X-ray diffraction spectra of LB film composed of PDA/Ag (50 nm, positive charge) composite vesicles. The inset shows the schematic illustration of the structure of this LB film

efficient PDA/Ag nanocomposite vesicles LB films are 0.09 and $1.92 \times 10^2 \text{ cm}^{-1}$, respectively. The nonlinear refractive index and the nonlinear absorption coefficient are measured to be $5.82 \times 10^{-12} \text{ cm}^2/\text{W}$ and $1.47 \times 10^{-9} \text{ m/W}$, respectively. Thus the resulting $\chi^{(3)}(\omega)$ were calculated to be $5.3 \times 10^{-10} \text{ esu}$. As the reference sample, the linear absorbance coefficient, the nonlinear refractive index, the nonlinear absorption coefficient, and $\chi^{(3)}(\omega)$ for pure PDA vesicles and PDA vesicles mixed with negatively charged nano-silver particles LB films were measured to be $3.15 \times 10^2 \text{ cm}^{-1}$, $2.45 \times 10^2 \text{ cm}^{-1}$, $9.16 \times 10^{-13} \text{ cm}^2/\text{W}$, $2.81 \times 10^{-12} \text{ cm}^2/\text{W}$, $4.53 \times 10^{-10} \text{ m/W}$, $5.89 \times 10^{-10} \text{ m/W}$, $7.1 \times 10^{-11} \text{ esu}$ and $2.3 \times 10^{-10} \text{ esu}$, respectively. All the values of n_2 , $\text{Re} \chi^{(3)}$ and nonlinear absorption coefficient for different samples were listed in Table 1. Obviously, LB films of PDA/Ag composite vesicles promoted NLO prop-

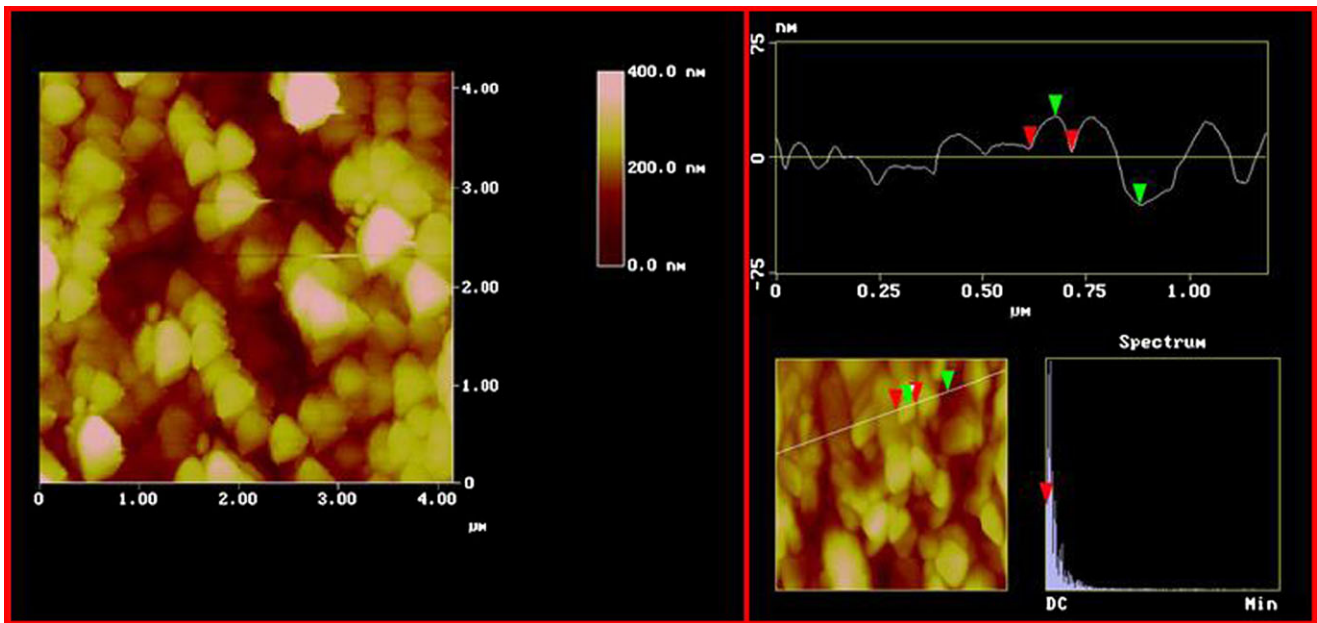
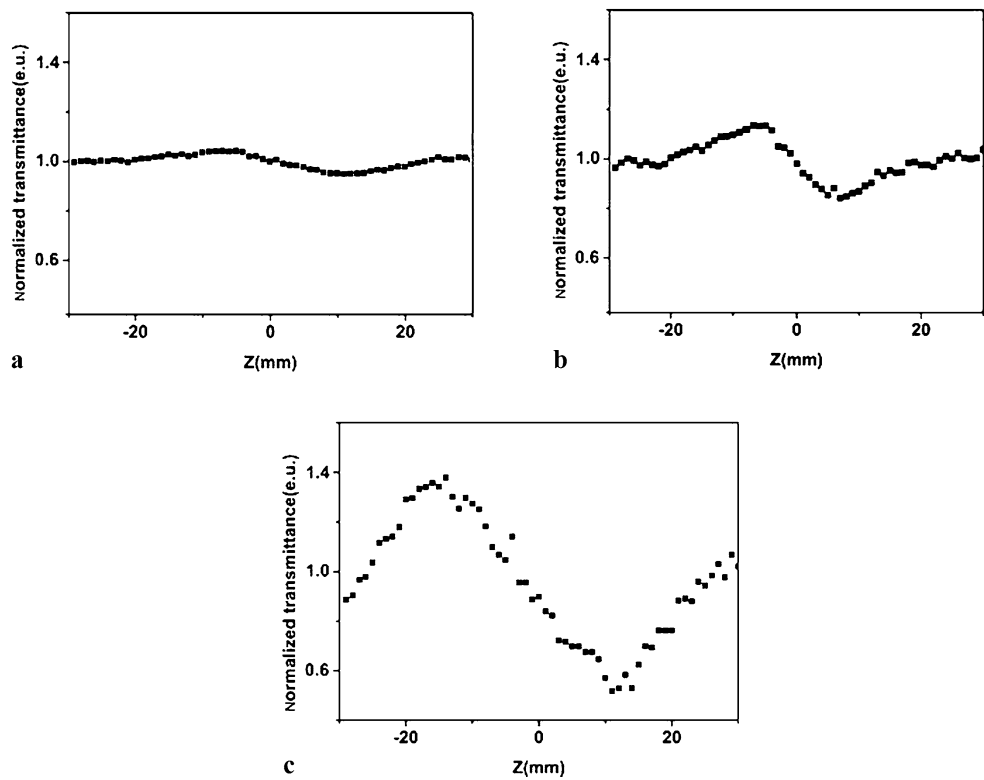


Fig. 8 AFM images showing the topography and the roughness profile along the *white line* indicated by the *green* and *red* arrows of LB films prepared from PDA/Ag (50 nm, positive charge) composite vesicles on glass substrate

Fig. 9 Measured Z-scan normalized transmittance curves of **a** pure PDA vesicles LB films (100 layers). **b** PDA vesicles mixed with Ag nanoparticles (50 nm, negative charge) LB films (100 layers). **c** PDA/Ag (50 nm, positive charge) nanocomposite vesicles LB films (100 layers)



erties enhancement. Compared to that of pure PDA vesicles LB films, the resulting $\chi^{(3)}(\omega)$ of LB films of PDA vesicles mixed with negatively charged nano-silver particles showed nearly 2.5 times enhancement, which should be ascribed to the local-field enhancement effect of loading of Ag

nano particles. However, the resulting $\chi^{(3)}(\omega)$ of PDA/Ag (50 nm) nanocomposite vesicles LB films showed nearly eight times enhancement compared to pure PDA vesicles LB films, and nearly 5000 times enhancement compared to that of pure PDA vesicles solution. This stupendous en-

hancement can be explained as follows: the spacing and relative position of the neighboring PDA/Ag composite vesicles in LB films were closer than those in solution, which would cause remarkable enhancement in NLO properties due to the coupling effect. The resulting $\chi^{(3)}(\omega)$ of PDA/Ag (50 nm) nanocomposite vesicles LB films was about 2.3 times larger than the value of LB films of PDA vesicles mixed with negatively charged nano-silver particles, which indicated that the optical nonlinearity is enhanced in the assembly of PDA/Ag core-shell structure due to the local-field enhancement effect. The local field could be concentrated in both the core and shell region of the nanocomposite vesicles at the surface-mediated plasma resonance. This increased field is then utilized for self-enhancements of the optical nonlinearity from each component of the composite films [15, 34]. Beside the huge NLO property, these NLO materials are also very stable for applications. All type of the LB films still have the same NLO susceptibility $\chi^{(3)}(\omega)$ after three months exposure in air. We anticipate that suitable immobilization spacing and relative position of the neighboring PDA/Ag composite vesicles in LB films should lead to more giant enhancements in third-order NLO response.

4 Conclusions

In summary, different size (20, 50 and 80 nm) Ag colloidal nanoparticles were coated onto the outer surface of polydiacetylene (PDA) vesicles to form PDA/Ag nanocomposite vesicles. Compared to pure PDA vesicles, the Ag colloidal nanoparticles coating led to the significant enhancement of NLO properties for PDA vesicles. Obviously, PDA/Ag (50 nm) composite vesicles showed maximum NLO properties enhancement effect (nearly 13 times) and this size-dependent enhancement effect of Ag colloidal nanoparticles can be attributed to mediation of a size-dependent light-confinement effect and a size-dependent dielectric constant of Ag spheres. The nonlinear properties of PDA/Ag nanocomposite vesicles can be easily modulated by varying the size, shape of Ag nanoparticles coated onto the outer surface of PDA vesicles. Further, these PDA vesicles were immobilized onto substrate to enhance their storage stability and user-friendliness. Obviously, these PDA/Ag composite vesicles LB film had dramatic NLO properties. The resulting $\chi^{(3)}(\omega)$ of PDA/Ag (50 nm) nanocomposite vesicles LB films showed nearly eight times enhancement compared to that of pure PDA vesicles LB films, and nearly 5000 times enhancement compared to that of pure PDA vesicles solution. Suitable immobilization spacing and relative position of the neighboring PDA/Ag composite vesicles is expected to lead to stupendous enhancements in third-order NLO response. Although the PDA/Ag nanocomposite vesicles LB film is still not sufficient for practical device applications,

the strategy described in this work still would be useful in the development of PDA-based optical and NLO devices. It is predictable that we will prepare the novel NLO optic material which is sufficient for device applications according to the optimization of different factors.

Acknowledgements This work was supported by the National Natural Science Foundation of China (No: 50703038, No: 50973101, No: 50533040, No: 50773075 and No: 50640420265), Specialized Research Fund for the Doctoral Program of Higher Education (No. 20070358065), National Basic Research Program of China (No. 2006cb302900) and Chinese Academy of Sciences (No. kjcx3.syw.H02).

References

1. S. Park, M. Pelton, M. Liu, P. Guyot-Sionnest, N.F. Scherer, *J. Phys. Chem. C* **111**, 116–123 (2007)
2. A. Sarkar, S. Okada, H. Matsuzawa, H. Matsuda, H. Nakanishi, *J. Mater. Chem.* **10**, 819 (2000)
3. F. D'Amore, A. Zappettini, G. Facchini, S.M. Pietralunga, M. Martinelli, C. Dell'Erba, C. Cuniberti, D. Comoretto, G. Dellepiane, *Synth. Met.* **127**, 143 (2002)
4. E. Giorgetti, G. Toci, M. Vannini, F. Giammanco, *Opt. Commun.* **217**(1–6), 431 (2003)
5. J.F. Zhang, Y.L. Song, J.Y. Yang, M.G. Humphrey, C. Zhang, *Cryst. Growth Des.* **8**, 387–390 (2008)
6. X. Kou, S. Zhang, Z. Yang, C.K. Tsung, G.D. Stucky, L. Sun, J. Wang, C. Yan, *J. Am. Chem. Soc.* **129**, 6402–6404 (2007)
7. M.A. van Dijk, M. Lippitz, M. Orrit, *Acc. Chem. Res.* **38**, 594–601 (2005)
8. S. Ohnishi, Y. Orimoto, F.L. Gu, Y. Aoki, *J. Chem. Phys.* **127**, 084702 (2007)
9. B. Champagne, B. Kirtman, *Handbook of Advanced Electronic and Photonic Materials and Devices* (Academic Press, New York, 2001)
10. Ch. Bosshard, K. Sutter, Ph. Prêtre, J. Hulliger, M. Flörshemer, P. Kaatz, P. Günter, in *Organic Nonlinear Optical Materials*, ed. by F. Kajzar, A.F. Garito. *Advances in Nonlinear Optics*, vol. 1 (Gordon and Breach, Basel, 1995), p. 89. Chap. 6
11. A. Masuhara, H. Kasai, T. Kato, S. Okada, H. Oikawa, Y. Nozue, S.K. Tripathy, H. Nakanishi, *J. Macromol. Sci., Pure Appl. Chem. A.* **38**(12), 1371 (2001)
12. R.E. Schwerzel, K.B. Spahr, J.P. Kurmer, V.E. Wood, J.A. Jenkins, *J. Phys. Chem. A.* **102**, 5622 (1998)
13. E. Giorgetti, G. Margheri, S. Sottini, M. Muniz-Miranda, *Synth. Met.* **139**, 929 (2003)
14. E. Shirai, Y. Urai, K. Itoh, *J. Phys. Chem. B.* **102**, 3765 (1998)
15. A.E. Neeves, M.H. Birnboim, *J. Opt. Soc. Am. B.* **6**, 787 (1989)
16. H.S. Zhou, T. Wada, H. Sasabe, *Appl. Phys. Lett.* **68**(9), 1288 (1996)
17. H.S. Zhou, T. Wada, H. Sasabe, H. Komiyama, *Synth. Met.* **81**, 129 (1996)
18. H. Katagi, H. Kasai, S. Okada, H. Oikawa, H. Matsuda, H. Nakanishi, *Polym. Adv. Technol.* **11**, 778 (2000)
19. W. Lu, W. Wang, Y. Su, J. Li, L. Jiang, *Nanotechnology* **16**, 2582 (2005)
20. T. Onodera, Z. Tan, A. Masuhara, H. Oikawa, H. Kasai, H. Nakanishi, T. Sekiguchi, *Jpn. J. Appl. Phys.* **45**(1), 379 (2006)
21. A.W. Olsen, Z.H. Kafafi, *J. Am. Chem. Soc.* **113**, 7758 (1991)
22. X. Chen, G. Zou, Y. Deng, Q.J. Zhang, *Nanotechnology* **19**, 195703 (2008)
23. H.B. Liao, R.F. Xiao, J.S. Fu, R. Yu, G.K.L. Wong, P. Sheng, *Appl. Phys. Lett.* **70**, 1 (1997)

24. K. Lance Kelly, Eduardo Coronado, Lin Lin Zhao, George C. Schatz, *J. Phys. Chem. B* **107**, 668–677 (2003)
25. Y. Deng, Ph.D. Thesis, University of Science and Technology of China, 2008
26. Y. Hamanaka, K. Fukuta, A. Nakamura, L.M. Liz-Marz'an, P. Mulvaney, *Appl. Phys. Lett.* **84**, 4938 (2004)
27. Y.L. Su, *J. Colloid Interface. Sci.* **292**, 271–276 (2005)
28. A. Potisatityuenyong, G. Tumcharern, S.T. Dubas, M. Sukwat-tanasinitt, *J. Colloid Interface. Sci.* **304**, 45–51 (2006)
29. Y.F. Yan, Ph.D. Thesis, University of Science and Technology of China, 2007
30. M. Sheik-Bahae, A.A. Said, T.H. Wei, D.J. Hagan, E.W. VanStry-land, *J. Quantum Electron.* **26**, 760 (1990)
31. K.L. Kelly, E. Coronado, L.L. Zhao, G.C. Schatz, *J. Phys. Chem. B* **107**, 668–677 (2003)
32. U. Kreibig, M. Vollmer, *Optical Properties of Metal Clusters* (Springer, Berlin, 1995)
33. T. Okamoto, M. Haraguchi, M. Fukui, *Jpn. J. Appl. Phys.* **43**(9), 6507–6512 (2004)
34. Y. Yang, M. Hori, T. Hayakawa, M. Nogami, *Surf. Sci.* **579**, 215–224 (2005)